Proteomic measures of gamma oscillations

Stephanie D. Byrum [a], Charity L. Washam [a], Alan J. Tackett [a], Edgar Garcia-Rill [b,*],
Veronica Bisagno [c], Francisco J. Urbano [d]

[a] Center for Translational Pediatric Research, Arkansas Children's Research Institute, Little Rock, AR, USA
[b] Center for Translational Neuroscience, University of Arkansas for Medical Sciences, Little Rock, AR, USA
[c] ININFA, Argentina
[d] IFIBYNE, CONICET, Universidad de Buenos Aires, Buenos Aires, Argentina

ARTICLE INFO

ABSTRACT

Background: Gamma oscillations serve complex processes, and the first stage of their generation is the reticular activating system (RAS), which mediates the gamma-activity states of waking and paradoxical sleep. We studied whether the pedunculopontine nucleus (PPN), part of the RAS in which every cell manifests intrinsic gamma oscillations, undergoes changes resulting in distinctive protein expression.

New method: We previously found that a histone deacetylation inhibitor, trichostatin A (TSA), acutely (30 min) blocked these oscillations. We developed a proteomic method for sampling stimulated and unstimulated PPN and determining protein expression in 1 mm punches of tissue from brain slices subjected to various treatments.

Results: We compared brain slices exposed for 30 min to TSA (unstimulated), to the cholinergic agonist carbachol (CAR), known to induce PPN gamma oscillations, or exposed to both TSA + CAR.

Comparison with existing methods: Label-free proteomics provides an unbiased and sensitive method to detect protein changes in the PPN. Our approach is superior to antibody-based methods that can lack specificity and can only be done for known targets. Proteomics methods like these have been leveraged to study molecular pathways in numerous systems and disease states.

Conclusions: Significant protein changes were seen in two functions essential to the physiology of the PPN: cytoskeletal and intracellular $[Ca^{2+}]$ regulation proteins. TSA decreased, while CAR increased, and TSA + CAR had intermediate effects, on expression of these proteins. These results support the feasibility of the methods developed for determining proteomic changes in small samples of tissue participating in the most complex of brain processes.

1. Introduction

Without high frequency beta/gamma activity there is no purposeful brain function. Without such activity there is no sensation, perception, memory, movement, thought, or action (Eckhorn et al., 1988; Gray and Singer, 1989; Jones, 2007; Llinas et al., 1991; Palva et al., 2009; Philips and Takeda, 2009; Singer, 1993; Voss et al., 2009). Low frequency activity in the brain at rest is ~10 Hz (alpha), the idling speed of the brain. If activity is slower, there is only sleep, nobody home. Without beta-/gamma activity, there is no consciousness (Garcia-Rill, 2015). Beta-/gamma activity in the reticular activating system (RAS), and specifically the pedunculopontine nucleus (PPN), is the first stage in which sensory input revs up brain activity, it has been termed "bottom-up gamma", responsible for setting the background of activity for sensation, perception, and waking (Garcia-Rill, 2017; Garcia-Rill et al., 2018). PPN high frequency activity is generated by high threshold, voltage-dependent calcium channels (the action of sodium and potassium channels in the PPN is simply too slow to generate such high frequency activity) (Kezunovic et al., 2011). This "bottom-up gamma" is relayed through the intralaminar thalamus and basal forebrain, and triggers cortical gamma band activity (Castro et al., 2013; Cavelli et al., 2017). Without "bottom-up gamma" there is no waking, no arousal, no cogent state upon which to decide to think or move. That is, without gamma oscillations, there is no thought or behavior.

A significant problem with proteomic and genomic analyses of the brain is the variety of cell types manifesting a myriad of receptors and a host of ionic channels. This makes it difficult to ascribe changes in protein levels and gene expression. In the current study, the preparation we

used employed blockers and tetrodotoxin (TTX) (same as when recording gamma oscillations, Kezunovic et al., 2011; Urbano et al., 2018) to ensure that fast synaptic transmission and circuit activity through action potentials was prevented. The activity present in the system, therefore, was mainly from intrinsic membrane oscillations, and limited to high frequency gamma oscillations mainly in cells manifesting P/Q-and N-type type channels. As such, proteomic and genomic changes may be more easily ascribed to specific processes related to the generation of gamma band activity.

The pedunculopontine nucleus (PPN) is the only nucleus in the RAS that is active during both states of high frequency (beta/gamma) EEG activity as in waking and REM sleep. Classic studies of recordings of PPN neurons during sleep-wake states revealed neurons that were active during waking and REM sleep, and none were active during slow wave sleep (Sakai et al., 1990; Steriade et al., 1990; Kayama et al., 1992; Datta and Siwek, 2002; Datta et al., 2009; Boucetta et al., 2014). Gamma band activity has been observed in the cortical EEG of the cat *in vivo* and in PPN neurons when the animal is active (Steriade et al., 1990). Additionally, in humans, gamma band activity has been shown in the region of the PPN during stepping, but not at rest (Fraix et al., 2008). Primates have also been observed to have PPN firing at low frequencies ~10 Hz at rest, but upon waking or walking on a treadmill firing is increased to gamma band frequencies (Goetz et al., 2016). Thus, the same cells were involved in both arousal and motor control in the PPN *in vitro*, *in vivo*, and across species, including man.

Our previous findings established that every PPN neuron fired maximally at beta/gamma frequencies (Simon et al., 2010), that all PPN neurons manifested beta/gamma frequency intrinsic membrane oscillations (Urbano et al., 2012), and that these oscillations were mediated only by high threshold, voltage-dependent N- and/or P/Q-type calcium channels (Kezunovic et al., 2011). We found that these channels were distributed along the dendrites of PPN neurons (Hyde et al., 2013), and that some cells exhibited both N- and P/Q-type calcium channels, some had only N-type channels, and some had only P/Q-type channels (Luster et al., 2015, 2016).

Our most recent results showed that, a) acute *in vitro* exposure to the histone deacetylation inhibitor trichostatin A (TSA) led to the elimination of high threshold, voltage-dependent Ca^{2+} channel-mediated intrinsic membrane oscillations, specifically in the gamma band range, but not lower frequency oscillations, b) pre-incubation with TSA led to a similar decrease specifically in gamma band oscillations, and c) a significant reduction in calcium currents was elicited by TSA (Urbano et al., 2018). These results suggest that there is a specific effect on gamma band oscillations when histone deacetylation is maximally blocked after >30 min. Thus, this work aims to develop a new method for determining proteomic changes in small samples of tissue. Changes in protein levels resulting from this newly described protocol can be correlated to previously described alterations in gamma oscillations (Kezunovic et al., 2013; Urbano et al., 2018).

2. Materials and methods

2.1. Slice preparation

Pups aged 9–13 days from adult timed-pregnant Sprague-Dawley rats (280–350 g) were anesthetized with ketamine (70 mg/kg, I.M.) until tail pinch reflex was absent. Pups were decapitated and the brain was rapidly removed then cooled in oxygenated sucrose-artificial cerebrospinal fluid (sucrose-aCSF). The sucrose-aCSF consisted of (in mM): 233.7 sucrose, 26 $NaHCO_3$, 3 KCl, 8 $MgCl_2$, 0.5 $CaCl_2$, 20 glucose, 0.4 ascorbic acid, and 2 sodium pyruvate. Sagittal sections (400 um) containing the PPN were cut and slices were allowed to equilibrate in normal aCSF at room temperature. Approximately 4 slices per brain contained the PPN. The aCSF was composed of (in mM): 117 NaCl, 4.7 KCl, 1.2 $MgCl_2$, 2.5 $CaCl_2$, 1.2 NaH_2PO_4, 24.9 $NaHCO_3$, and 11.5 glucose. Slices were then incubated at 36 °C while perfused (1.5 ml/min) with oxygenated (95% O_2- 5% CO_2)

aCSF. During incubation, aCSF solution contained the following synaptic receptor antagonists: the selective NMDA receptor antagonist 2-amino-5-phosphonovaleric acid (APV, 40 μM), the competitive AMPA/kainate glutamate receptor antagonist 6-cyano-7-nitroquinoxaline-2,3-dione (CNQX, 10 μM), the glycine receptor antagonist strychnine (STR, 10 μM), the specific GABA-A receptor antagonist gabazine (GBZ, 10 μM), and the nicotinic receptor antagonist mecamylamine (MEC, 10 μM) collectively referred to here as synaptic blockers (SB). We also used the sodium channel blocker tetrodotoxin (TTX, 3 μM).

These conditions mimicked those used for PPN patch clamp recording studies of intrinsic gamma oscillations (Simon et al., 2010; Garcia-Rill et al., 2011; Kezunovic et al., 2011; Hyde et al., 2013; Luster et al., 2015, 2016; Urbano et al., 2014, 2018), allowing us to analyze PPN intrinsic properties and their role on gamma oscillations in total isolation from synaptic inputs from their surrounding network of cells. All experimental protocols were approved by the Institutional Animal Care and Use Committee of the University of Arkansas for Medical Sciences and were in agreement with the "Guidelines for the Care and Use of Mammals in Neuroscience and Behavioral Research'', used by the National Institutes of Health for the care and use of laboratory animals.

2.2. Incubation or stimulation

Slices containing the PPN were incubated in aCSF (unstimulated), and compared to slices incubated with the cholinergic agonist carbachol (CAR 50 μM) (stimulated), and each group was incubated in TSA for 30 min, providing TSA, CAR, and TSA + CAR groups. Exposure to CAR is known to induce gamma oscillations in PPN neurons (Kezunovic et al., 2013), and is a well-known agent for activating PPN (for review see Garcia-Rill, 2015). We based our working concentrations of HDAC inhibitors on previously published reports using neurons in vitro (Akhtar et al., 2009; Calfa et al., 2012). Trichostatin A (TSA) at 1 μM was higher than the lowest effective concentration used on dopaminergic neurons in vitro (Hsu et al., 2016). That is, based on the differential affinities, the final concentration used was 1 μM for TSA (6.5x IC_{50}), which was established as effective and without deleterious effects in our previous studies (Urbano et al., 2018). No changes were observed after TSA (1 μM) acute administration in voltage-dependence of calcium current I–V curves (Urbano et al., 2018). Furthermore, TSA's rapid effects in vitro might be due to the acetylation of multiple proteins located outside the nucleus (Choudhary et al., 2009). Indeed, we have suggested that alterations in the acetylation/deacetylation equilibrium may blunt the Ca^{2+}-CAM kinase II homeostatic modulation of P/Q-type calcium channels (Urbano et al., 2018; Garcia-Rill et al., 2019). The stock solution of TSA was dissolved in DMSO and immediately stored at -30 °C. The final concentration of DMSO in the incubation aCSF solution was <0.01%. Control aCSF contained the same DMSO concentration as in control unstimulated conditions. Slices were floated onto sterile petri dishes and 1 mm punch biopsies taken of the PPN under a dissection microscope at x10. Biopsies were immediately inserted into sterile microcentrifuge tubes and frozen in dry ice.

2.3. Proteomics

Brain slices from three animals per condition (total of 11 slices per condition) were analyzed by high resolution mass spectrometry. We used triplicate samples for the proteomics analysis. Extracted proteins were reduced, alkylated, and digested using filter-aided sample preparation (Wisniewski et al., 2009). Tryptic peptides were then separated by reverse phase XSelect CSH C18 2.5 um resin (Waters) on an in-line 150 × 0.075 mm column using an UltiMate 3000 RSLCnano system (Thermo Scientific). Peptides were eluted using a 90 min gradient from 97:3 to 60:40 buffer A (0.1% formic acid, 0.5% acetonitrile):B (0.1% formic acid, 99.9% acetonitrile) ratio. Eluted peptides were ionized by electrospray (2.15 kV) followed by MS/MS analysis using higher-energy collisional dissociation (HCD) on an Orbitrap Fusion Lumos mass spectrometer

(Thermo Scientific) in top-speed data-dependent mode. MS data were acquired using the FTMS analyzer in profile mode at a resolution of 240, 000 over a range of 375–1500 m/z. Following HCD activation, MS/MS data were acquired using the ion trap analyzer in centroid mode and normal mass range with precursor mass-dependent normalized collision energy between 28.0 and 31.0.

Proteins were identified by searching against the UniprotKB database restricted to Rattus (July 2018 database; 8047 protein entries) using Mascot (Matrix Science; version 2.5.1). Search parameters included fixed modification set as carbamidomethyl on C, variable modifications set as oxidation on M and acetyl on peptide N-terminal, parent ion tolerance of 3 ppm and a fragment ion tolerance of 0.5 Da. Scaffold (Proteome Software) was used to verify MS/MS based peptide and protein identifications. Peptide identifications were accepted if they could be established with less than 1.0% false discovery by the Scaffold Local FDR algorithm. Protein identifications were accepted if they could be established with less than 1.0% false discovery and contained at least 2 identified peptides. Protein probabilities were assigned by the Protein Prophet algorithm (Nesvizhskii et al., 2003).

Protein spectral counts were filtered so at least one sample had 5 or more spectral counts, replaced missing values with 0.5, normalized the counts to the normalized spectral abundance factor (NSAF) as described in (Zybailov et al., 2006), and log2 transformed the data. The NSAF formula is as follows: NSAF = (spectral count/protein molecular weight)/sum of (spectral counts/molecular weight). The sum included the SC/MW for all proteins within the same sample. NSAF normalization accounts for differences in larger and smaller proteins. Larger proteins have a higher probability of detecting peptides vs smaller proteins and therefore normalizing based on the length or molecular weight accounts for this discrepancy. A student's t-test and fold change were calculated using the log2 NSAF transformed data. We also provide ANOVA p-values with Tukey post-hoc multiple comparisons test for comparing each sample group. The full proteomics results are provided in Supplementary Table 1. Proteins were considered significant with a p-value < 0.05. Data visualization images were generated using Venny (version 2.1) for the Venn Diagrams showing proteins identified, Bioconductor package ComplexHeatmap in R, and plot function in R for the volcano plots.

3. Results

3.1. Population response recordings

Our previous studies using TSA found that either acute or prolonged exposure to TSA reduced or eliminated intrinsic gamma oscillations in single PPN neurons (Urbano et al., 2018). Such patch clamp studies typically employ fast synaptic blockers (SBs) and tetrodotoxin (TTX), such as used herein, for taking biopsies from the PPN. We carried out a small study to determine the effects of TSA on slices without SBs and TTX. The question is, does CAR induce gamma oscillations in the population as a whole, and does TSA affect that network activity? We recorded population responses from the PPN in slices stimulated by CAR (50 μM) before and after exposure to TSA. Recordings were amplified with a Grass Inst. (Quincy, MA) P511 amplifier, filtered at 1Hz-1KHz, and digitized with a Digidata-1440 at a rate of 10 kHz. Averages of recordings and power spectra were analyzed using pClamp10 software. Further analysis was conducted using MatLab software (The MathWorks, Natick, MA). Plots of the event related spectral perturbation (ERSP) for each population response were generated with the EEGLAB MatLab Toolbox (Delorme and Makeig, 2004). CAR was superfused for 10 min before TSA was added for 10 min, and then CAR was continued without TSA for another 10 min Fig. 1 shows four brainstem slice population response recordings from the PPN before and after TSA exposure. The ERSPs (left side) are running power spectra over time from PPN population recordings in a slice before (pre) and after (post) TSA exposure for 10 min. The power spectra on the right are cumulative spectra for the entire 10 min. In both ERSP and power spectra, it was clear that CAR alone (black record)

induced a peak at gamma band frequencies (~35–40 Hz), while CAR after TSA (red record) showed markedly decreased gamma band activity. Changes in activity at other frequencies were variable. These results suggest that the gamma band activity known to be induced in PPN population response recordings by CAR (Simon et al., 2010; Garcia-Rill et al., 2011) is markedly reduced by exposure to TSA.

3.2. Proteomics characterization

In order to identify the protein changes within the PPN due to TSA and CAR exposure, we employed high resolution mass spectrometry. Protein lysates were prepared from triplicate samples in four groups: untreated brain slices, treated with TSA or CAR alone, and TSA in combination with CAR. Protein lysates from the PPN were trypsin digested into peptides using filter-aided sample preparation (FASP) (Wisniewski et al., 2009). The peptides were separated on an in line reverse phase LC column and peptides were eluted over a 90 min gradient. The spectra were searched against the UniprotKB database restricted to Rattus in Mascot. A total of 2,702 proteins were identified from all samples; however, after filtering for low spectral counts (required at least one sample with 5 or more spectral counts), a total of 1,721 proteins were analyzed for differential expression. Of these identified proteins, 99.4% of the proteins were present in all four groups (Supplementary Table 1).

After filtering, the spectral counts were normalized to Log2 NSAF for differential expression. A student's t-test was used to calculate p-values for three different comparisons: 1) Untreated vs TSA, 2) Untreated vs CAR, and 3) Untreated vs TSA plus CAR to investigate protein changes in TSA and CAR alone and in combination. Proteins with a p-value < 0.05 were considered significant. Of these, only 3.7% were significant in all comparisons, regardless of treatment. There were 18.7%, 24.8%, and 36.1% significant proteins unique to each comparison: untreated PPN to TSA, CAR, and TSA plus CAR, respectively (Supplementary Table 2).

A hierarchical cluster was generated using the Bioconductor package ComplexHeatmap in R. The log2 NSAF values for proteins found to be significantly differentially expressed by a p-value < 0.05 are visualized and show clear separation of the sample groups; untreated vs TSA, untreated vs CAR, and untreated vs TSA plus CAR. TSA treatment had the least amount of protein changes whereas the combination treatment had the most. There were 101, 135, and 170 significant proteins for TSA, CAR, and TSA plus CAR, respectively (Fig. 2, Supplementary Table 3).

Volcano plots help visualize the protein changes for each group comparison; untreated vs TSA (Fig. 3A), untreated vs CAR (Fig. 3B), and untreated vs TSA plus CAR (Fig. 3C). The $\log_2$ fold change (x-axis) and $-\log_{10}$ p-value (y-axis) of each protein identified in each of the comparisons is shown. Significant proteins that are either up- or down-regulated in the treatment are highlighted in red and blue, respectively. The horizontal line indicates a p-value of 0.05.

4. Discussion

4.1. Caveats

We utilized a label-free proteomic workflow to provide an unbiased and sensitive method to detect protein changes in the PPN. This approach is superior to antibody-based, protein detection methods that can lack specificity and can only be done for known targets in a lower throughput manner. Proteomics methods, like the one used in this study, have been leveraged to study molecular pathways in numerous systems and disease states. For example, we have used similar approaches to characterize molecular pathways in cancer (Byrum et al., 2013). Proteomics studies on tissues can have cell specific limitations when the tissue sample is limited and single cells cannot be isolated in enough abundance for proteomic analysis. Here we circumvent that limitation by taking advantage of specific blockers of gamma band oscillations (i.e., using concentrations of TSA previously described to acutely block gamma
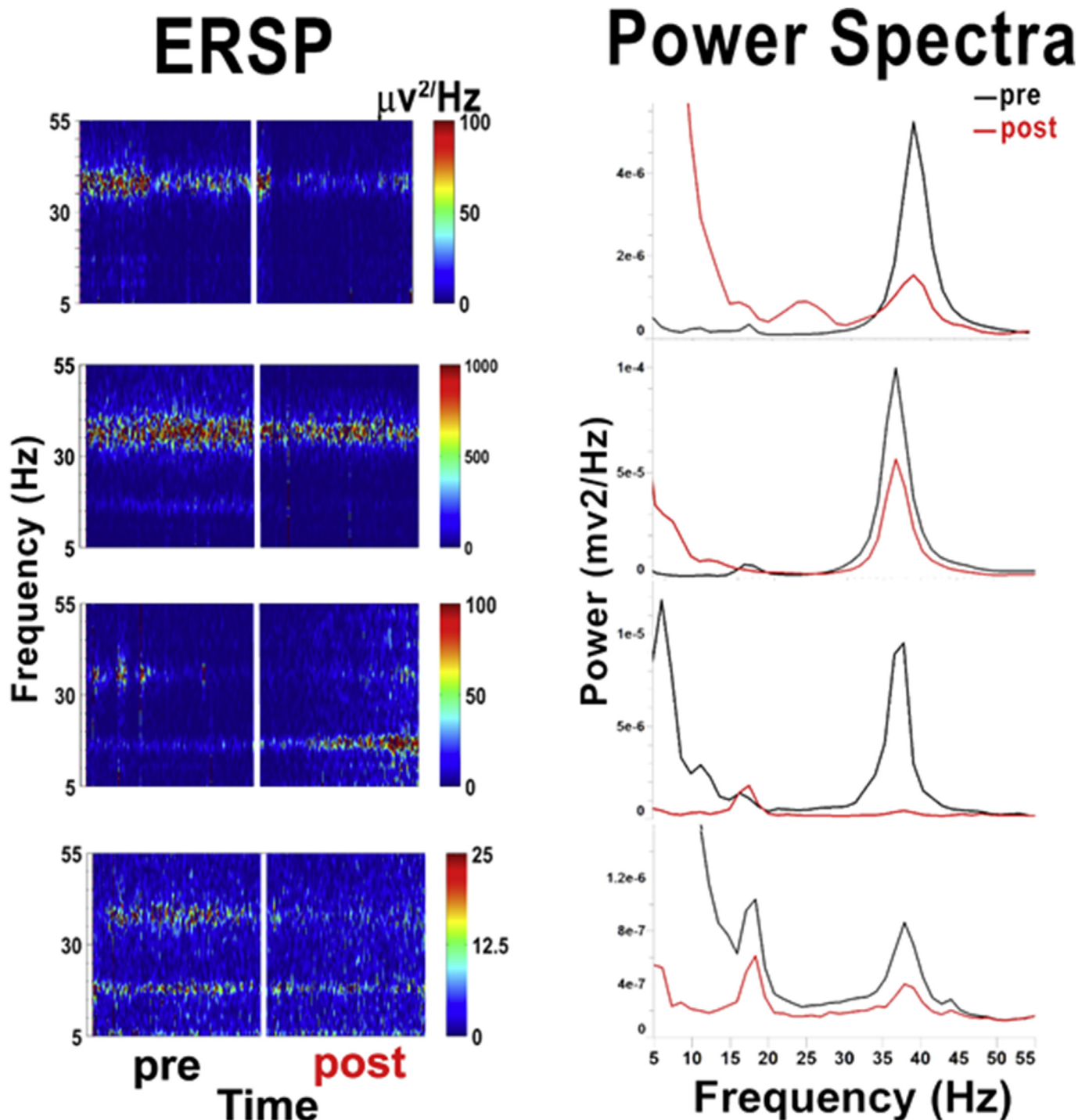
Fig. 1. Population responses in PPN. Left side. Population response recordings using low resistance (1–2 MΩ) electrodes in four individual slices containing the PPN shown in ERSP form. Recordings shown were collected from different slices. Briefly, exposure to CAR before (pre) TSA showed significant levels of activity in the beta/gamma range during the initial 10 min. After 10 min of TSA (not shown) it was discontinued, and CAR was superfused for another 10 min after TSA (post). In all cases, gamma frequency activity was reduced and lower frequency activity became more pronounced, at least in some cases, but not all. These results suggest that TSA reduced gamma band activity in the PPN network, despite being stimulated by CAR.

oscillation).

While our method appears to yield quite specific results on protein expression, there are a number of other issues that need to be addressed. Indeed, the proteins changes reported in this study require further support by alternative experimental means. In addition, the effects of TSA are fairly broad and long lasting. Therefore, exposure for only 30 min would seem to potentiate any lack of specificity. The fact that there were a number of quite specific changes in protein expression would argue

against an unspecific influence. Moreover, our previous studies showed that the inhibitory effects of TSA on gamma oscillations began within minutes, and they were mirrored by inhibition of histone deacetylase (HDAC) IIa using MC1568, but there was no effect when MS275 was used to block HDAC I (Urbano et al., 2018). That is, a targeted action on HDAC IIa appeared responsible for the decrease in gamma activity. We also used 30 min pre-incubations with TSA to determine if longer exposure would have the same effects, which was indeed what was found, and the effects
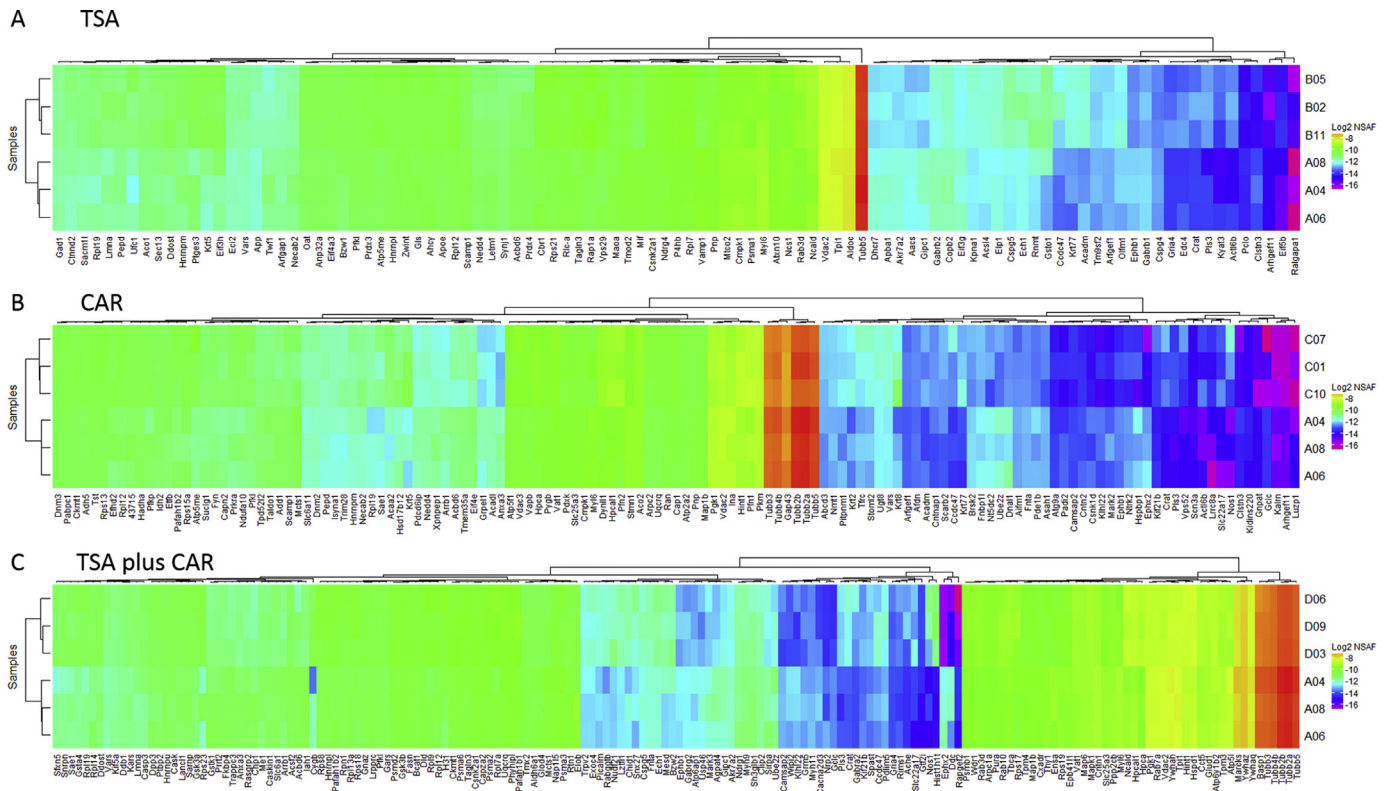
Fig. 2. Hierarchical clustering of differentially expressed proteins from exposure to TSA, CAR, and TSA + CAR. The $\log_2$ NSAF values are shown for significantly differentially expressed proteins between the untreated samples and TSA (A), CAR Act16b (B), and combination treatment with TSA + CAR (C). Proteins were considered significant with a t-test p-value < 0.05. The combination exposure had the most impact on the proteome.

were not potentiated or more widespread. In addition, those studies employed synaptic blockers and sodium channel blockade, as well as ramp stimuli, permitting only high threshold calcium channel-mediated gamma oscillations. That is, there was no other activity present and thus only gamma oscillations were affected by TSA and MC1568, but not MS275. Population responses demonstrated that gamma band activity was preferentially affected by TSA (Fig. 1). The results of the present study, like those of our previous work (Urbano et al., 2018), demonstrated changes in protein expression within minutes, but there certainly are changes that occur within hours or perhaps days after TSA exposure. While this is an acceptable pursuit, we are interested in the acute effects of TSA, which is known to have soporific effects on patients, and its inhibition of gamma oscillations, which could certainly account for this fairly rapid side effect.

Another issue is whether TSA is acting directly on the calcium channels being studied. Previous results showed that calcium currents were affected mostly in the plateau phase and not the early rapid phase mediated by other types of calcium channels (Urbano et al., 2018), suggesting not all calcium channels were affected. Moreover, we previously reported that it was PPN cells with P/Q-type calcium channels and not N-type calcium channels in which gamma oscillation inhibition was inhibited by TSA (Urbano et al., 2018). Interestingly, the present results suggest that CAR, when exposed along with TSA, had intermediate effects, showing that the two agents competed for PPN cell activity. If TSA acted directly on P/Q-type calcium channels, CAR would not demonstrate competitive effects since it acts on cholinergic receptors. The results rather point to a balance between synaptic and intrinsic activity modulating the action of PPN neurons intracellularly. Moreover, our
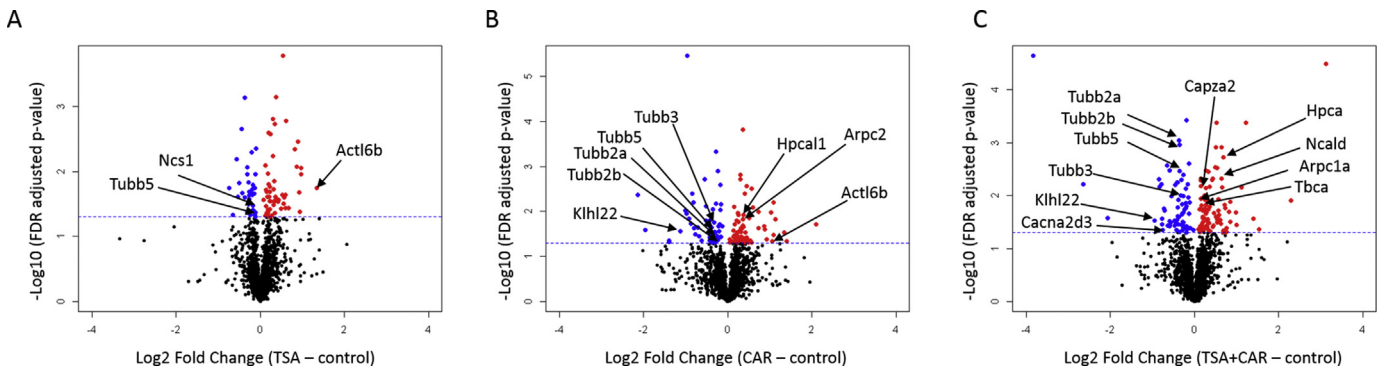
Fig. 3. Volcano plots depicting protein expression in each of the treatments; TSA (A), CAR (B), and TSA + CAR (C). The $\log_2$ fold change (x-axis) and $-\log_{10}$ p-value (y-axis) of each protein identified in each of the comparisons is shown. Significant proteins that are either up- or down-regulated in the treatment are highlighted in red and blue, respectively. The horizontal line indicates a p-value of 0.05.

previous study established that CaMKII blockade decreased the oscillations, once again pointing to an intracellular site of action (Urbano et al., 2018). The question is, what is that intracellular mechanism by which TSA and MC1568 affect gamma oscillations?

Interestingly, the most significant protein changes observed involved two neuronal functions, known to be essential to the physiology of the PPN: cytoskeletal and intracellular [Ca^{2+}] regulation. Interestingly, acute treatment with TSA + CAR altered a considerably larger number of proteins, up- and down-regulating their levels, compared to acute TSA treatment alone. Interestingly, CAR treatment augmented proteins levels of actin-like proteins that increased actin polymerization. Understanding whether these protein changes underlined the effects of TSA vs. TSA + CAR, or represented mechanisms of molecular compensation for the cellular and physiological consequences of those treatments remains to be elucidated.

4.2. Cytoskeleton

One interesting outcome of this work was the observed changes in abundance of several proteins related to the actin cytoskeleton. Actin and tubulin proteins are known to be functionally interrelated. Understanding actin-tubulin interactions is essential to describing how neuronal compartments integrate synaptic inputs with their intrinsic properties (Coles and Bradke, 2015). Acute treatment with TSA increased actin-like protein 6B, a nuclear protein involved in transcriptional activation and repression of select genes by chromatin remodeling (Wu et al., 2007), while decreasing the levels of F-actin capping protein beta, an inhibitor F-actin polymerization (Coles and Bradke, 2015). These changes are particularly important since F-actin bundles exert force on the plasma membrane, stabilizing ion channel membrane expression while interacting with tubulin microtubules (Coles and Bradke, 2015). TSA + CAR treatment increased actin-related protein 2/3 levels, which is known to induce actin polymerization (Welch et al., 1997). TSA + CAR treatment also decreased several tubulin and actin associated proteins. As mentioned above, altering F-actin protein levels would have a significant impact on CaMKII-dependent gamma activity maintenance through its direct involvement in CaMKII-beta and alpha subunit dimerization (Shen et al., 1998), and their intracellular translocation (Shen and Meyer, 1999). Furthermore, TSA + CAR treatment decreased the level of a Kelch-like protein. Kelch-like proteins have been shown to positively modulate P/Q-type calcium channel activity (Aromolaran et al., 2007; Perissinotti et al., 2014). In agreement, the acute effects of TSA on PPN rhythmicity were found to be mediated by an intracellular CaMKII-dependent pathway (Urbano et al., 2018), and both TSA and CAR have been previously found to blunt P/Q-type channel-mediated calcium currents (Kezunovic et al., 2013; Urbano et al., 2018). In conclusion, TSA was able to altered key cytoskeletal proteins levels and membrane voltage-gated channels, which would result in a significant blunting of PPN physiology. These results are in agreement with previously described acetylation changes in cytoskeleton proteins by SAHA and MS275 HDAC inhibitors (Choudhary et al., 2009).

4.3. Intracellular [Ca^{2+}] regulation

TSA + CAR treatment boosted the levels of several proteins related to intracellular [Ca^{2+}] regulation like hippocalcin. Hippocalcin is a protein that acts as a sensor of intracellular [Ca^{2+}] transients after binding to the plasma membrane (Tzingounis et al., 2007). Neurocalcin protein levels were increased by acute treatment with TSA and TSA + CAR. Neurocalcin is a plasma-binding intracellular [Ca^{2+}] sensor that facilitates the slow after hyperpolarization of the neuronal membrane potential (Béven et al., 2010), allowing for the normal recovery of membrane potential after massive activation of voltage-gated calcium channels (e.g., after the sustained activation of PPN gamma oscillations).

Acute TSA treatment also reduced the levels of neuronal calcium sensor 1 (NCS-1), a [Ca^{2+}] sensor over-expressed in the brain of bipolar

disorders patients (Garcia-Rill et al., 2018), that has been observed to modulate gamma band oscillations in PPN neurons (D'Onofrio et al., 2015). acute TSA + CAR treatment down-regulated the voltage-dependent calcium channel $\alpha_2\delta$ subunit, an auxiliary subunit known to support the membrane trafficking of P/Q-type calcium channels (Klugbauer et al., 2003).

In summary, the method developed can sample physiologically relevant proteins involved in gamma band activity, which serves the most complex of brain processes. These analyses provide detailed results that help identify intracellular mechanisms involved in the acute regulation and proteomics of gamma band activity.

Declarations

Author contribution statement

Stephanie D. Byrum: Analyzed and interpreted the data; Wrote the paper.

Charity L. Washam: Analyzed and interpreted the data.

Alan J. Tackett: Conceived and designed the experiments; Analyzed and interpreted the data; Contributed reagents, materials, analysis tools or data; Wrote the paper.

Edgar Garcia-Rill: Conceived and designed the experiments; Performed the experiments; Analyzed and interpreted the data; Contributed reagents, materials, analysis tools or data; Wrote the paper.

Veronica Bisagno, Francisco J. Urbano: Conceived and designed the experiments; Performed the experiments; Analyzed and interpreted the data.

Competing interest statement

The authors declare no conflict of interest.

Additional information

Supplementary content related to this article has been published online at https://doi.org/10.1016/j.heliyon.2019.e02265.

References

Akhtar, M.W., Raingo, J., Nelson, E.D., Montgomery, R.L., Olson, E.N., Kavalali, E.T., Monteggia, L.M., 2009. Histone deacetylases 1 and 2 form a developmental switch that controls excitatory synapse maturation and function. J. Neurosci. 29 (25), 8288–8297.

Aromolaran, K.A., Benzow, K.A., Koob, M.D., Piedras-Rentería, E.S., 2007. The Kelch-like protein 1 modulates P/Q-type calcium current density. Neuroscience 145 (3), 841–850.

Béven, L., Adenier, H., Kichenama, R., Homand, J., Redeker, V., Le Caer, J.P., Ladant, D., Chopineau, J., 2010. Ca2+-myristoyl switch and membrane binding of chemically acylated neurocalcins. Biochemistry 40 (27), 8152–8160.

Boucetta, S., Cisse, Y., Mainville, L., Morales, M., Jones, B.E., 2014. Discharge profiles across the sleep-waking cycle of identified cholinergic, gabaergic, and glutamatergic neurons in the pontomesencephalic tegmentum of the rat. J. Neurosci. 34, 4708–4727.

Byrum, S.D., Larson, S.K., Avaritt, N.L., Moreland, L.E., Mackintosh, S.G., Cheung, W.L., Tackett, A.J., 2013. Quantitative proteomics identifies activation of hallmark pathways of cancer in patient melanoma. J. Proteom. Bioinform. 6 (3), 43–50.

Calfa, G., Chapleau, C.A., Campbell, S., Inoue, T., Morse, S.J., Lubin, F.D., Pozzo-Miller, L., 2012. HDAC activity is required for BDNF to increase quantal neurotransmitter release and dendritic spine density in CA1 pyramidal neurons. Hippocampus 22 (7), 1493–1500.

Castro, S., Falconi, A., Chase, M.H., Torterolo, P., 2013. Coherent neocortical 40-Hz oscillations are not present during REM sleep. Eur. J. Neurosci. 37, 1330–1339.

Cavelli, M., Castro-Zaballa, S., Mondino, A., Gonzalez, J., Falconi, A., Torterolo, P., 2017. Absence of EEG gamma coherence in a local activated neocortical state: a conserved trait of REM sleep. Transl. Brain Rhytmicity 2, 1–13.

Choudhary, C., Kumar, C., Gnad, F., Nielsen, M.L., Rehman, M., Walther, T.C., Olsen, J.V., Mann, M., 2009. Lysine acetylation targets protein complexes and co-regulates major cellular functions. Science 325 (5942), 834–840.

Coles, C.H., Bradke, F., 2015. Coordinating neuronal actin-microtubule dynamics. Curr. Biol. 25, R677–R6791.

Datta, S., Siwek, D.F., 2002. Single cell activity patterns of pedunculopontine tegmentum neurons across the sleep-wake cycle in the freely moving rats. J. Neurosci. Res. 70, 79–82.

Datta, S., Siwek, D.F., Stack, E.C., 2009. Identification of cholinergic and non-cholinergic neurons in the pons expressing phosphorylated cyclic adenosine monophosphate response element-binding protein as a function of rapid eye movement sleep. Neuroscience 163, 397–414.

Delorme, A., Makeig, S., 2004. EEGLAB: an open source toolbox for analysis of single-trial EEG dynamics including independent component analysis. J. Neurosci. Methods 134, 9–21.

D'Onofrio, S., Kezunovic, N., Hyde, J.R., Luster, B., Messias, E., Urbano, F.J., Garcia-Rill, E., 2015. Modulation of gamma oscillations in the pedunculopontine nucleus by neuronal calcium sensor protein-1: relevance to schizophrenia and bipolar disorder. J. Neurophysiol. 113 (3), 709–719.

Eckhorn, R., Bauer, R., Jordan, W., Brosch, M., Kruse, W., et al., 1988. Coherent oscillations: a mechanism of feature linking in the visual system? Biol. Cybern. 60, 121–130.

Fraix, V., Bastin, F., David, O., Goetz, L., Ferraye, M., et al., 2008. Pedunculopontine nucleus area oscillations during stance, stepping and freezing in Parkinson's disease. PLoS One 8, e83919.

Garcia-Rill, E., 2015. Waking and the Reticular Activating System. Academic Press, New York, p. 330.

Garcia-Rill, E., 2017. Bottom-up gamma and stages of waking. Med. Hypotheses 104, 58–62.

Garcia-Rill, E., D'Onofrio, S., Mahaffey, S.C., Bisagno, V., Urbano, F.J., 2019. Bottom-up gamma and bipolar disorder, clinical and neuroepigenetic implications. Bipolar Disord. 21 (2), 108–116.

Garcia-Rill, E., Mahaffey, S., Hyde, J.R., Urbano, F.J., 2019. Bottom-up gamma maintenance in various disorders. Neurobiol. Dis. 128, 31–39.

Garcia-Rill, E., Simon, C., Smith, K., Kezunovic, N., Hyde, J., 2011. The pedunculopontine tegmental nucleus: arousal from slices to humans: implications for DBS. J. Neural Transm. 118, 1397–1407.

Gray, C.M., Singer, W., 1989. Stimulus-specific neuronal oscillations in orientation columns of cat visual cortex. Proc. Nat. Acad. Sci. USA 86, 1698–1702.

Goetz, L., Piallat, B., Bhattacharjee, M., Mathieu, H., David, O., et al., 2016. The primate pedunculopontine nucleus region: towards a dual role in locomotion and waking state. J. Neural Transm. 123, 667–678.

Hsu, C.W., Shou, D., Huang, R., Khuc, T., Dai, S., et al., 2016. Identification of HDAC inhibitors using a cell-based HDAC I/II assay. J. Biomol. Screen 21, 643–652.

Hyde, J., Kezunovic, N., Urbano, F.J., Garcia-Rill, E., 2013. Spatiotemporal properties of high speed calcium oscillations in the pedunculopontine nucleus. J. Appl. Physiol. 115, 1402–1414.

Jones, E.G., 2007. Calcium channels in higher-level brain function. Proc. Nat. Acad. Sci. USA 14, 17903–17904.

Kayama, Y., Ohta, M., Jodo, E., 1992. Firing of 'possibly' cholinergic neurons in the rat laterodorsal tegmental nucleus during sleep and wakefulness. Brain Res. 569, 210–220.

Kezunovic, N., Hyde, J., Goitia, B., Bisagno, V., Urbano, F.J., et al., 2013. Muscarinic modulation of high frequency oscillations in pedunculopontine neurons. Front. Neurol. 4, 176.

Kezunovic, N., Urbano, F.J., Simon, C., Hyde, J., Smith, K., et al., 2011. Mechanism behind gamma band activity in the pedunculopontine nucleus (PPN). Eur. J. Neurosci. 34, 404–415.

Klugbauer, N., Marais, E., Hofmann, F., 2003. Calcium channel alpha2delta subunits: differential expression, function, and drug binding. J. Bioenerg. Biomembr. 35 (6), 639–647.

Llinas, R.R., Grace, A.A., Yarom, Y., 1991. In vitro neurons in mammalian cortical layer 4 exhibit intrinsic oscillatory activity in the 10- to 50-Hz frequency range. Proc. Nat. Acad. Sci. USA 88, 897–901.

Luster, B., D'Onofrio, S., Urbano, F.J., Garcia-Rill, E., 2015. High-Threshold $Ca2+$ channels behind gamma band activity in the pedunculopontine nucleus (PPN). Phys. Rep. 3, e12431.

Luster, B., Urbano, F.J., Garcia-Rill, E., 2016. Intracellular mechanisms modulating gamma band activity in the pedunculopontine nucleus (PPN). Phys. Rep. 4, e12787.

Nesvizhskii, A.I., Keller, A., Kolker, E., Aebersold, R., 2003. A statistical model for identifying proteins by tandem mass spectrometry. Anal. Chem. 75 (17), 4646–4658.

Palva, S., Monto, S., Palva, J.M., 2009. Graph properties of synchronized cortical networks during visual working memory maintenance. Neuroimage 49, 3257–3268.

Perissinotti, P.P., Ethington, E.G., Cribbs, L., Koob, M.D., Martin, J., Piedras-Rentería, E.S., 2014. Down-regulation of endogenous KLHL1 decreases voltage-gated calcium current density. Cell Calcium 55 (5), 269–280.

Philips, S., Takeda, Y., 2009. Greater frontal-parietal synchrony at low gamma-band frequencies for inefficient then efficient visual search in human EEG. Int. J. Psychophysiol. 73, 350–354.

Sakai, K., El Mansari, M., Jouvet, M., 1990. Inhibition by carbachol microinjections of presumptive cholinergic PGO-on neurons in freely moving cats. Brain Res. 527, 213–223.

Shen, K., Meyer, T., 1999. Dynamic control of CaMKII translocation and localization in hippocampal neurons by NMDA receptor stimulation. Science 284, 162–166.

Shen, K., Teruel, M.N., Subramanian, K., Meyer, T., 1998. CaMKIIbeta functions as an F-actin targeting module that localizes CaMKIIalpha/beta heterooligomers to dendritic spines. Neuron 21, 593–606.

Simon, C., Kezunovic, N., Ye, M., Hyde, J., Hayar, A., et al., 2010. Gamma band unit activity and population responses in the pedunculopontine nucleus. J. Neurophysiol. 104, 463–474.

Singer, W., 1993. Synchronization of cortical activity and its putative role in informtion processing and learning. Annu. Rev. Physiol. 55, 349–374.

Steriade, M., Paré, D., Datta, S., Oakson, D., Curro Dossi, R., 1990. Different cellular types in mesopontine cholinergic nuclei related to ponto-geniculo-occipital waves. J. Neurosci. 10, 2560–2579.

Tzingounis, A.V., Kobayashi, M., Takamatsu, K., Nicoll, R.A., 2007. Hippocalcin gates the calcium activation of the slow afterhyperpolarization in hippocampal pyramidal cells. Neuron 53 (4), 487–493.

Urbano, F.J., Kezunovic, N., Hyde, J., Simon, C., Beck, P., et al., 2012. Gamma band activity in the reticular activating system (RAS). Front. Neurol. Sleep Chronobiol. 3 (6), 1–16.

Urbano, F.J., D'Onofrio, S.M., Luster, B.R., Hyde, J.R., Bosagno, V., et al., 2014. Pedunculopontine nucleus gamma band activity- preconscious awareness, waking, and REM sleep. Front. Sleep Chronobiol. 5, 210.

Urbano, F.J., Bisagno, V., Mahaffey, S., Lee, S.-H., Garcia-Rill, E., 2018. Class II histone deacetylases require P/Q-type Ca^{2+} channels and CaMKII to maintain gamma oscillations in the pedunculopontine nucleus. Sci. Rep. 8, 13156.

Voss, U., Holzmann, R., Tuin, I., Hobson, J.A., 2009. Lucid dreaming: a state of consciousness with features of both waking and non-lucid dreaming. Sleep 32, 1191–1200.

Welch, M.D., DePace, A.H., Verma, S., Iwamatsu, A., Mitchison, T.J., 1997. The human Arp2/3 complex is composed of evolutionarily conserved subunits and is localized to cellular regions of dynamic actin filament assembly. J. Cell Biol. 138 (2), 375–384.

Wisniewski, J.R., Zougman, A., Nagaraj, N., Mann, M., 2009. Universal sample preparation method for proteome analysis. Nat. Methods 6, 359–362.

Wu, J.I., Lessard, J., Olave, I.A., Qiu, Z., Ghosh, A., Graef, I.A., Crabtree, G.R., 2007. Regulation of dendritic development by neuron-specific chromatin remodeling complexes. Neuron 56 (1), 94–108.

Zybailov, B., Mosley, A.L., Sardiu, M.E., Coleman, M.K., Florens, L., Washburn, M.P., 2006. Statistical analysis of membrane proteome expression changes in Saccharomyces cerevisiae. J. Proteome Res. 5 (9), 2339–2347.